Electrostatic Wave Decay in the Randomly Inhomogeneous Solar Wind

C. Krafft, P. Savoini

The Astrophysical Journal Letters, 964:L30 (8pp), 2024 April 1 https://doi.org/10.3847/2041-8213/ad3449

Electrostatic Wave Decay in the Randomly Inhomogeneous Solar Wind

C. Krafft[1,2] and P. Savoini[1]
[1] Laboratoire de Physique des Plasmas (LPP), CNRS, Sorbonne Université, Observatoire de Paris, Université Paris-Saclay, Ecole polytechnique, Institut Polytechnique de Paris, 91120 Palaiseau, France; catherine.krafft@universite-paris-saclay.fr
[2] Institut Universitaire de France (IUF), France
Received 2023 December 12; revised 2024 March 6; accepted 2024 March 11; published 2024 March 27

Abstract

Despite a few space observations where Langmuir and ion acoustic waves are expected to participate in the mechanism of electrostatic decay, this is to date believed to be the main and fastest nonlinear wave process in the solar wind. However, in such a plasma where random density fluctuations are ubiquitous, the question of whether nonlinear wave processes play a significant role in Langmuir wave turbulence generated by electron beams associated with type III solar radio bursts remains still open. This paper provides several answers by studying, owing to two-dimensional challenging particle-in-cell simulations, the dynamics and the properties of the ion acoustic waves excited by such Langmuir wave turbulence and the role they play in the electrostatic decay. The impact on this process of plasma background density fluctuations and electron-to-ion temperature ratio is studied. Moreover, it is shown that, for a typical solar wind plasma with an average level of density fluctuations of a few percent of the ambient density and a temperature ratio of the order of 1, nonlinear induced scattering off ions occurs, with small intensity low-frequency quasi-modes and only in localized plasma regions where density is depleted or weakly perturbed by low-frequency turbulence.

Unified Astronomy Thesaurus concepts: Solar electromagnetic emission (1490); Solar wind (1534); Radio bursts (1339); Solar flares (1496)

1. Introduction

Waveforms containing the beating signature of two high-frequency waves were first observed upstream of the foreshock of Jupiter (Gurnett et al. 1981) and, later, of the Earth (e.g., Kellogg et al. 1999). In some cases, such observations were associated with type III solar radio bursts (Gurnett et al. 1993; Hospodarsky & Gurnett 1995). An interpretation of the beating waves as signatures of nonlinear three-wave decay was proposed by Cairns & Robinson (1992), arguing that the two high-frequency peaks correspond to the beam-driven Langmuir waves $\mathcal{L}$ and the backscattered ones $\mathcal{L}'$, produced via the resonant electrostatic decay (ESD) $\mathcal{L} \rightarrow \mathcal{L}' + \mathcal{S}'$, where $\mathcal{S}'$ are ion acoustic waves (e.g., Tsytovich 1970; Melrose 1986). More recently, such double-peak features were observed by several satellites together with low-frequency emissions, with the authors arguing for ESD (Henri et al. 2009; Graham & Cairns 2013; Kellogg et al. 2013).

However, another interpretation was also proposed, presenting the double peak as a beam-driven incident Langmuir wave and its reflection on a density gradient (Willes et al. 2002). The solar wind indeed involves random density fluctuations δn of a few percent of the ambient plasma density n_0 (Celnikier et al. 1987; Krasnoselskikh et al. 2007; Krupar et al. 2020), that have a strong impact on the propagation of Langmuir waves and can be the cause of their conversion into electromagnetic waves (Kellogg et al. 1999; Krasnoselskikh et al. 2011; Volokitin & Krafft 2018). Due to the difficulty to distinguish the origin of a double-peak structure (a three-wave interaction process or wave scattering on plasma density fluctuations), the question of whether nonlinear processes play a significant role in Langmuir wave turbulence generated by electron beams during type III radio bursts in the solar wind remains open and still actively debated (e.g., Soucek et al. 2005). Moreover, in the framework of such radio bursts, the generation of backscattered Langmuir waves is of highest importance, as they participate to wave coalescence processes leading to harmonic electromagnetic wave radiation at frequency $2\omega_p$, whereas ion acoustic waves $\mathcal{S}'$ produced via ESD can stimulate the production of ion acoustic waves $\mathcal{S}$ (Robinson et al. 1994) involved in the electromagnetic decay $\mathcal{L} \rightarrow \mathcal{F} + \mathcal{S}$ supposed to lead to the radiation of electromagnetic waves $\mathcal{F}$ at frequency ω_p (e.g., Tsytovich 1970; Melrose 1986).

In homogeneous plasmas, ESD has been studied in one-dimensional (1D) geometry, using Vlasov codes (Umeda & Ito 2008; Henri et al. 2009) or weak turbulence equations (Kontar & Pécseli 2002; Li et al. 2003) but never particle-in-cell (PIC) simulations, except, to our knowledge, for particular cases considering nonpropagating backscattered $\mathcal{L}'$ waves (Sauer et al. 2017) or wave backscattering (Nishikawa & Cairns 1991) in a homogeneous plasma. Moreover, ESD was studied using Zakharov's equations (Krafft et al. 2015, 2019) in 1D plasmas with and without applied random density fluctuations.

In this Letter we study the ESD $\mathcal{L} \rightarrow \mathcal{L}' + \mathcal{S}'$ in homogeneous and randomly inhomogeneous plasmas, with different electron-to-ion temperature ratios T_e/T_i and average levels of density fluctuations $\Delta N = (\langle(\delta n/n_0)^2\rangle)^{1/2}$, for conditions typical of type III solar radio bursts near 1 au (e.g., Reid & Ratcliffe 2014, and references therein, Krupar et al. 2015; Dakeyo et al. 2022; Wilson et al. 2023). For the first time, two objectives are reached owing to large-scale and long-term challenging 2D PIC simulations, i.e., (i) to show the occurrence of 2D ESD in a homogeneous plasma by presenting in detail the low-frequency waves' dynamics and characteristics (spectra, dispersion, energy growth, saturation,

and damping), as well as relevant signatures of their nonlinear interactions with Langmuir waves (resonance conditions, waves' phase correlations, space and time cross-bicoherences), and (ii) to study the dependence of the decay process as a function of ΔN and T_e/T_i, in order to state if, in an actual solar wind plasma with $\Delta N \sim 0.05$ and $T_e/T_i \sim 1$, ESD can be the dominant process, or if the linear conversion of Langmuir waves on density fluctuations is the main source of backscattered Langmuir waves. Whereas ESD is to date considered the main and fastest nonlinear wave interaction process in homogeneous plasmas with developed Langmuir wave turbulence, this statement has to be seriously reconsidered in actual solar wind plasmas where random density fluctuations are ubiquitous and ion acoustic damping is significant.

2. Simulation Results

A 2D3V version of the relativistic full electromagnetic PIC code SMILEI is used (Derouillat et al. 2017). Simulations involve 1800 macroparticles per cell and per each of the three species (plasma ions and electrons, beam electrons) in order to minimize the numerical noise below the average levels $\Delta N = 0.025$ and 0.05 of the external density fluctuations, of the order of a few percent of the background plasma density n_0 (Krafft & Savoini 2021, 2022). These initially applied random inhomogeneities evolve self-consistently during the simulations. The drift and thermal velocities of the type III beam considered are $v_b \simeq 0.25c$ and $v_{T_b} = v_T$, where v_T is the electron plasma thermal velocity. The weak beam relative density, $n_b/n_0 = 5 \times 10^{-4}$, enables us to work in the kinetic instability regime. The beam is injected parallel to the x-axis with a 2D Maxwellian velocity distribution function (Krafft & Savoini 2023).

PIC simulations are performed for conditions typical of type III solar radio source regions near 1 au (e.g., Reid & Ratcliffe 2014, and references therein), considering homogeneous ($\Delta N = 0$) and randomly inhomogeneous plasmas ($\Delta N = 0.025,\ 0.05$), with electron-to-ion temperature ratios $T_e/T_i = 1$ and 10, which delimit the range of actual solar wind temperature ratios near 1 au (Dakeyo et al. 2022; Wilson et al. 2023). The lengths of the simulation box are $L_x = L_y = 1448\lambda_D$; λ_D is the electron Debye length. The mass ratio is $m_i/m_e = 1836$; m_i and m_e are the proton and electron masses. The weak solar wind magnetic field is neglected.

The characteristic wavenumber $k_{\mathcal{L}}$ of the beam-driven Langmuir waves along the beam direction is $k_{\mathcal{L}}\lambda_D \sim 0.1$. The simulations are performed up to $t = 15,000\omega_p^{-1}$, in order to obtain very long time series necessary for the identification of the low-frequency waves. The study of ESD is a challenging task that requires us to follow simultaneously the dynamics of high- and low-frequency waves, whose frequencies unfold over 3 orders of magnitude.

The ESD of beam-driven Langmuir waves, i.e., $\mathcal{L} \rightarrow \mathcal{L}' + \mathcal{S}'$ (e.g., Tsytovich 1970; Melrose 1986), leads to the generation of backscattered Langmuir waves $\mathcal{L}'$ and forward propagating ion acoustic waves $\mathcal{S}'$. The resonance conditions are $\omega_{\mathcal{L}} = \omega_{\mathcal{L}'} + \omega_{\mathcal{S}'}$, with $\boldsymbol{k}_{\mathcal{L}} = \boldsymbol{k}_{\mathcal{L}'} + \boldsymbol{k}_{\mathcal{S}'}$, where ω and $\boldsymbol{k}$ refer to frequencies and wavevectors. In a homogeneous plasma, the Langmuir and ion acoustic wave dispersion relations are $\omega_{\mathcal{L}}/\omega_p \simeq 1 + 3\boldsymbol{k}_{\mathcal{L}}^2\lambda_D^2/2$ and $\omega_{\mathcal{S}'} \simeq c_s k_{\mathcal{S}'}$ where $c_s = ((T_e + 3T_i)/m_i)^{1/2}$.

In 1D geometry, the above resonance conditions lead to $\boldsymbol{k}_{\mathcal{S}'} \simeq (2|\boldsymbol{k}_{\mathcal{L}}| - k_0)\boldsymbol{e}_L$ and $\boldsymbol{k}_{\mathcal{L}'} \simeq (k_0 - |\boldsymbol{k}_{\mathcal{L}}|)\boldsymbol{e}_L$, where $k_0 = 2\omega_p c_s/3v_T^2 \ll |\boldsymbol{k}_{\mathcal{L}}|$, $|\boldsymbol{k}_{\mathcal{L}'}|$ and $\boldsymbol{e}_L = \boldsymbol{k}_{\mathcal{L}}/|\boldsymbol{k}_{\mathcal{L}}|$ (Robinson et al. 1993). Depending on the value of k_0, the second decay cascade $\mathcal{L}' \rightarrow \mathcal{L}'' + \mathcal{S}''$ can occur, where $\mathcal{S}''$ is a backward propagating ion acoustic wave and $\mathcal{L}''$ is a forward propagating Langmuir wave, with wavevectors $\boldsymbol{k}_{\mathcal{S}''} \simeq (-2|\boldsymbol{k}_{\mathcal{L}}| + 3k_0)\boldsymbol{e}_L$ and $\boldsymbol{k}_{\mathcal{L}''} \simeq (|\boldsymbol{k}_{\mathcal{L}}| - 2k_0)\boldsymbol{e}_L$, deduced from the three-wave resonance conditions $\boldsymbol{k}_{\mathcal{L}'} = \boldsymbol{k}_{\mathcal{L}''} + \boldsymbol{k}_{\mathcal{S}''}$ and $\omega_{\mathcal{L}'} = \omega_{\mathcal{L}''} + \omega_{\mathcal{S}''}$ in 1D geometry (e.g., Li et al. 2003; Krafft et al. 2015). These wavevector values can be used as estimates for the case of 2D geometry.

2.1. Homogeneous Plasma

Figure 1(a) presents the time variations of the energies (i) $W_{\mathcal{L}}$, $W_{\mathcal{L}'}$, and $W_{\mathcal{L}''}$ of the Langmuir waves $\mathcal{L}$, $\mathcal{L}'$, and $\mathcal{L}''$, and (ii) $W_{\mathcal{S}'}$ and $W_{\mathcal{S}''}$ of the ion acoustic waves $\mathcal{S}'$ and $\mathcal{S}''$. Whereas $W_{\mathcal{L}}$ increases due to beam instability, the energies $W_{\mathcal{L}'}$ ($W_{\mathcal{L}''}$) and $W_{\mathcal{S}'}$ ($W_{\mathcal{S}''}$), involved in the same decay process, reach their maxima roughly at the same time $\omega_p t \sim 5000$ ($\omega_p t \sim 10{,}000$). Note the very large time domain (up to $15{,}000\omega_p^{-1}$) allowing us to observe simultaneously the growth and the saturation stages of all the high- and low-frequency waves involved in the first and the second decay cascades. The Langmuir wave spectrum is shown at time $\omega_p t = 4500$ when $W_{\mathcal{S}'}$ reaches its maximum (Figure 1(b)). Beam-driven Langmuir waves $\mathcal{L}$ are excited near $k_{x\mathcal{L}}\lambda_D \sim 0.1$ whereas $\mathcal{L}'$ ($\mathcal{L}''$) propagate with $k_{x\mathcal{L}'} < 0$ ($k_{x\mathcal{L}''} > 0$). The spatial distribution of the normalized ion density perturbations $\delta n_i/n_0$ can be observed at the same time in Figure 1(c). Their wavelength $\lambda_{\mathcal{S}'} \simeq 35\lambda_D$, observed almost ubiquitously, corresponds to ion acoustic waves $\mathcal{S}'$ with $|\boldsymbol{k}_{\mathcal{S}'}| \simeq 2|\boldsymbol{k}_{\mathcal{L}}|$ ($k_0 \simeq 0.017$), suggesting that the ESD $\mathcal{L} \rightarrow \mathcal{L}' + \mathcal{S}'$ occurs in the whole simulation box. Moreover, Figure 1(d) shows the spatiotemporal cross-distribution (at fixed y) of $\delta n_i/n_0$ up to $\omega_p t \simeq 15{,}000$, exhibiting the presence of $\mathcal{S}'$ and $\mathcal{S}''$ waves revealed by descending and ascending lines, spaced by distances equal to the ion acoustic wavelengths ($\lambda_{\mathcal{S}'} \simeq 2\pi/(2|\boldsymbol{k}_{\mathcal{L}}| - k_0) \simeq 35\lambda_D$, $\lambda_{\mathcal{S}''} \simeq 2\pi/|(-2|\boldsymbol{k}_{\mathcal{L}}| + 3k_0)| \simeq 42\lambda_D$), and propagating with opposite group velocities c_s/v_T and $-c_s/v_T$.

Figure 2 shows the energy spectra of ion acoustic waves at three times before the saturation of their energy near $\omega_p t \simeq 6000$, together with their dispersion curves (ω, k_x), to which the theoretical ones are superimposed. At $\omega_p t = 1500$, forward propagating waves $\mathcal{S}'$ produced by the decay $\mathcal{L} \rightarrow \mathcal{L}' + \mathcal{S}'$ appear near $k_x\lambda_D \simeq 0.18$, as expected by theory, as well as, starting from $\omega_p t = 2500$, backward propagating waves $\mathcal{S}''$ produced by the second decay cascade $\mathcal{L}' \rightarrow \mathcal{L}'' + \mathcal{S}''$. Dispersion curves show, at $k_x > 0$, the excitation of $\mathcal{S}'$ waves near $\omega/\omega_p \simeq 0.005$ (maximum of intensity), corresponding to the expected value $k_x\lambda_D \simeq 0.18$. Finally, at $\omega_p t = 4500$, the two spectral domains corresponding to ion acoustic waves produced by the first and second decay cascades are clearly visible, as well as on the dispersion curves. Note the low-frequency excitation near $k_x \sim 0$, also visible in 1D studies (Krafft et al. 2015) or weak turbulence studies (Ziebell et al. 2015), concerning waves of large wavelengths that do not play a role in the processes studied here.

In order to demonstrate that three-wave interaction actually takes place, we present in Figures 3(a)–(b) the space and time cross-bicoherences b_c (Kim & Powers 1979) calculated using the electric fields' components E_x and E_y as well as the ion density perturbation δn_i associated with the waves participating in the three-wave process

$$b_c(X_1, X_2) = \frac{|\langle \delta n_i(X_1) E_x(X_2) E_y^*(X_1 + X_2)\rangle|}{(\langle |\delta n_i(X_1)|^2 |E_x(X_2)|^2\rangle \langle |E_y^*(X_1 + X_2)|^2\rangle)^{1/2}},$$

where the brackets denote ensemble averaging; (X_1, X_2) are the parallel wavenumbers (k_{x1}, k_{x2}) or frequencies (ω_1, ω_2), at the time

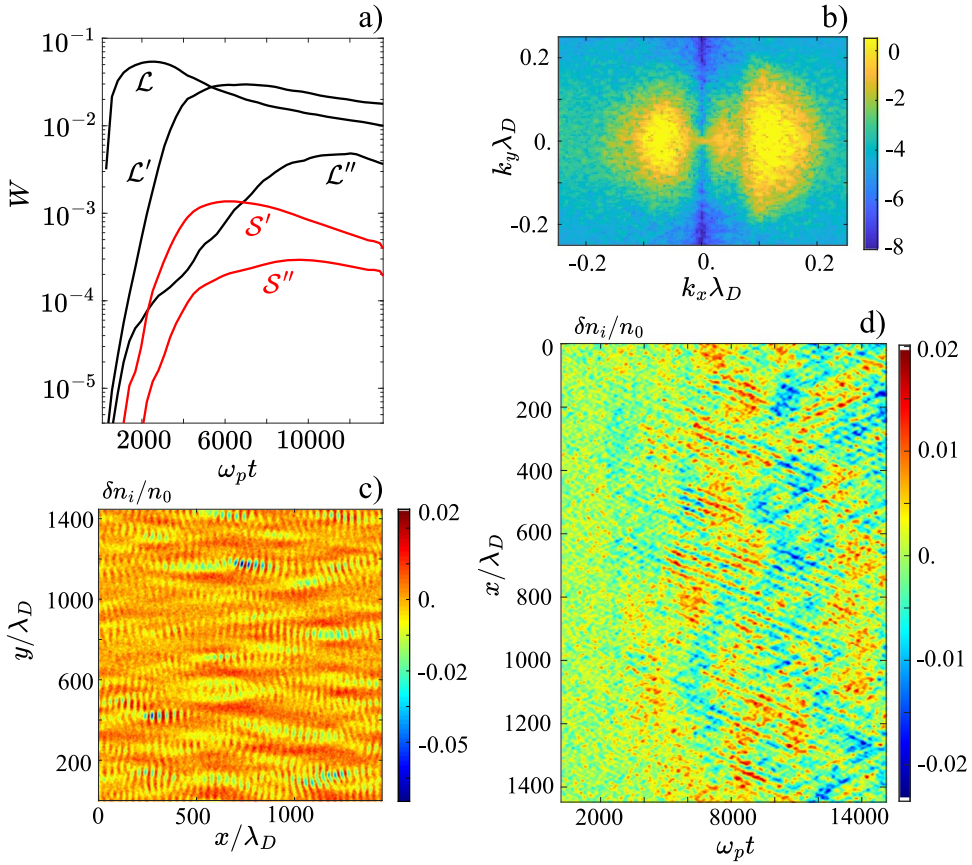

Figure 1. Homogeneous plasma with $T_e/T_i = 10$. (a) Time variations of energies (integrated on the 2D simulation box and normalized by the beam initial energy) of Langmuir waves $\mathcal{L}$, $\mathcal{L}'$, and $\mathcal{L}''$, and ion acoustic waves $\mathcal{S}'$ and $\mathcal{S}''$, in logarithmic scale. (b) Langmuir wave energy spectrum in the plane $(k_x\lambda_D, k_y\lambda_D)$, at $\omega_p t = 4500$, in logarithmic scale. (c) Space distribution of $\delta n_i/n_0$, at $\omega_p t = 4500$, in the plane $(x/\lambda_D, y/\lambda_D)$. (d) Spatiotemporal variation of the cross-distribution along x (at fixed y) of $\delta n_i/n_0$, with descending and ascending lines exhibiting the propagation of waves $\mathcal{S}'$ and $\mathcal{S}''$, with group velocities $-c_s/v_T$ and c_s/v_T. All variables are normalized.

$\omega_p t = 4500$ corresponding to Langmuir (Figure 1(b)) and ion acoustic waves' spectra (Figure 2). In Figure 3(b), the highest level of cross-bicoherence is $b_c(k_{x1},\ k_{x2}) = 0.86$, at $k_{x1} = k_{x\mathcal{S}'} = 0.225\lambda_D^{-1}$ ($0.14 \lesssim k_{x\mathcal{S}'}\lambda_D \lesssim 0.24$; Figure 2) and $k_{x2} = k_{x\mathcal{L}'} = -0.096\lambda_D^{-1}$ ($-0.12 \lesssim k_{x\mathcal{L}'}\lambda_D \lesssim -0.03$; Figure 1(b)). In Figure 3(a), the maximum is $b_c(\omega_1,\ \omega_2) = 0.5$, at $\omega_1 = \omega_{\mathcal{S}'} = 0.006\omega_p^{-1}$ and $\omega_2 = \omega_{\mathcal{L}'} = 1.014\omega_p^{-1}$. It implies that $\omega_{\mathcal{L}} = 1.020\omega_p^{-1}$, which corresponds for parallel propagation to $k_{x\mathcal{L}} \simeq 0.117\lambda_D^{-1}$, not far from $k_{x\mathcal{S}'} + k_{x\mathcal{L}'} = 0.129\lambda_D^{-1}$. However, as propagation is not strictly parallel, i.e., $k_{y1} = k_{y\mathcal{S}'} = 0.06\lambda_D^{-1}$ and $k_{y\mathcal{L}'} = -0.06\lambda_D^{-1}$ (see spectra of Figures 1(b) and 2 within regions of highest intensity) satisfying $k_{y\mathcal{L}} = k_{y\mathcal{L}'} + k_{y\mathcal{S}'}$ with $k_{y\mathcal{L}} \sim 0$, we obtain that $\omega_{\mathcal{L}'} = 1.019\omega_p^{-1}$ and $\omega_{\mathcal{S}'} = 0.0061\omega_p^{-1}$, so that $\omega_{\mathcal{L}} = \omega_{\mathcal{L}'} + \omega_{\mathcal{S}'} = 1.025\omega_p^{-1}$, which corresponds, due to dispersion, to $k_{x\mathcal{L}} = 0.129\lambda_D^{-1} = k_{x\mathcal{L}'} + k_{x\mathcal{S}'}$, which is satisfied with high accuracy. This demonstrates that the resonance conditions $\omega_{\mathcal{L}} = \omega_{\mathcal{L}'} + \omega_{\mathcal{S}'}$ and $\boldsymbol{k}_{\mathcal{L}} = \boldsymbol{k}_{\mathcal{L}'} + \boldsymbol{k}_{\mathcal{S}'}$ are fulfilled when the nonlinear interaction between the waves takes place.

Moreover, Figure 3(c) shows the time variations of energies $W_{\mathcal{L}}$, $W_{\mathcal{L}'}$, and $W_{\mathcal{S}'}$, as well as of energy products $W_{\mathcal{L}}W_{\mathcal{S}'}$ and $W_{\mathcal{L}}W_{\mathcal{L}'}$. For the ratio $T_e/T_i = 10$ considered here, ion acoustic waves are weakly damped and we can use the method employed in our previous works (Krafft & Savoini 2021, 2022) that, on the basis of energy conservation of a three-wave system, allows us to find a signature of this nonlinear interaction by showing that the time growth of the energy of one wave is proportional to the growth of the product of the two other waves energies. One observes that $W_{\mathcal{L}}W_{\mathcal{S}'} \propto W_{\mathcal{L}'}$ (light blue dotted line follows blue line) and $W_{\mathcal{L}}W_{\mathcal{L}'} \propto W_{\mathcal{S}'}$ (pink dotted line follows red line) during the growth stages of $\mathcal{L}'$ and $\mathcal{S}'$ waves ($\omega_p t \lesssim 5000$). Such result, together with the waves' phase correlations highlighted by the cross-bicoherence, confirms the occurrence of a three-wave nonlinear interaction. Finally, let us apply this procedure to the time variations of energies $W_{\mathcal{L}'}$, $W_{\mathcal{L}''}$, and $W_{\mathcal{S}''}$ and energy products $W_{\mathcal{L}''}W_{\mathcal{S}''}$ and $W_{\mathcal{L}''}W_{\mathcal{L}'}$. We observe that $W_{\mathcal{L}''}W_{\mathcal{S}''} \propto W_{\mathcal{L}'}$ (green dotted line follows black line) and $W_{\mathcal{L}''}W_{\mathcal{L}'} \propto W_{\mathcal{S}''}$ (pink dotted line follows red line) during the growth of $\mathcal{S}''$ waves ($\omega_p t \lesssim 5000$), confirming that the process observed is the second decay cascade $\mathcal{L}' \rightarrow \mathcal{L}'' + \mathcal{S}''$. In conclusion, both decay cascades are shown to be three-wave interaction mechanisms, in conditions relevant to type III solar radio bursts.

In 3D geometry, at the saturation of the ESD, the occupation numbers $N_{\mathcal{L}}$ and $N_{\mathcal{S}'}$ of $\mathcal{L}$ and $\mathcal{S}'$ waves (Tsytovich 1970)

$$N_{\mathcal{L}} \simeq \frac{(2\pi)^3 w_{\mathcal{L}}}{\omega_{\mathcal{L}} k_{\mathcal{L}}^2 \Delta k_{\mathcal{L}} \Delta\Omega_{\mathcal{L}}}, \qquad N_{\mathcal{S}'} \simeq \frac{(2\pi)^3 w_{\mathcal{S}'}}{\omega_{\mathcal{S}'} k_{\mathcal{S}'}^2 \Delta k_{\mathcal{S}'} \Delta\Omega_{\mathcal{S}'}},$$

have to satisfy $N_{\mathcal{S}'} \simeq N_{\mathcal{L}}$, where $w_{\mathcal{L}}$ and $w_{\mathcal{S}'}$ are the energy densities of the $\mathcal{L}$ and $\mathcal{S}'$ waves. Considering that solid angles satisfy $\Delta\Omega_{\mathcal{S}'} \simeq \Delta\Omega_{\mathcal{L}}$ (Robinson et al. 1993), one can write at saturation that $W_{\mathcal{S}'}/W_{\mathcal{L}} \simeq w_{\mathcal{S}'}/w_{\mathcal{L}} \simeq (\omega_{\mathcal{S}'}/\omega_{\mathcal{L}})(k_{\mathcal{S}'}^2/k_{\mathcal{L}}^2)(\Delta k_{\mathcal{S}'}/\Delta k_{\mathcal{L}})$, which can be applied in our 2D geometry case. With $k_{\mathcal{S}'} \simeq 2k_{\mathcal{L}}$ (see above), $\Delta k_{\mathcal{S}'} \simeq \Delta k_{\mathcal{L}}$, and $\omega_{\mathcal{S}'}/\omega_p \simeq 0.006$ (see Figure 2),

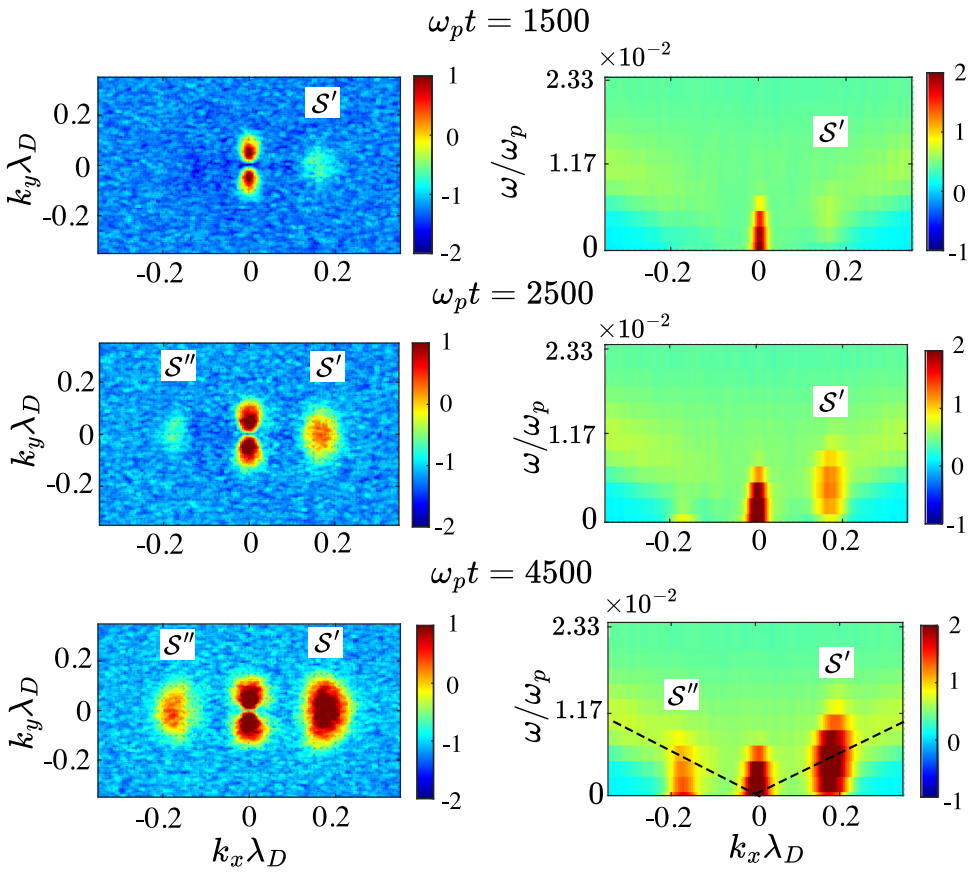

Figure 2. Homogeneous plasma with $T_e/T_i = 10$. (Left column) Ion acoustic energy spectra in the plane $(k_x\lambda_D, k_y\lambda_D)$, at $\omega_p t = 1500$, 2500, and 4500, in logarithmic scale. (Right column) Ion acoustic dispersion curves, at the same times, in the plane $(\omega/\omega_p, k_x\lambda_D)$; the black dashed lines represent the theoretical dispersion law. All variables are normalized. Labels indicate the ion acoustic waves $\mathcal{S}'$ and $\mathcal{S}''$.

one obtains the theoretical estimate $(W_{\mathcal{S}'}/W_{\mathcal{L}})_{\rm th} \simeq 0.025$. On the other hand, using the time variations of wave energies (Figure 1(a)), one finds $W_{\mathcal{S}'}/W_{\mathcal{L}} \simeq 0.02$–$0.03$ (depending on the time chosen in the saturation stage), in good agreement with $(W_{\mathcal{S}'}/W_{\mathcal{L}})_{\rm th}$, showing that the saturation condition expected for ESD is recovered by the simulations and that the decay process identified behaves as expected by theory.

2.2. Impact of Random Density Fluctuations

Let us now study the impact of applied random density fluctuations of average level ΔN on the decay process. For an inhomogeneous plasma with $\Delta N = 0.05$, Figures 4(a)–(d) show, at $\omega_p t = 2500$ and $\omega_p t = 4500$, the energy spectra and the dispersion curves of the ion acoustic waves excited. Despite significant wave scattering and broadening, one can identify these modes on dispersion curves (and wave spectra) even if, compared to the homogeneous plasma case, the latter are no more well shaped but strongly scattered, with amplitudes at least one decade less. At $\omega_p t = 2500$, dispersion curves show the excitation of $\mathcal{S}'$ waves around $k_{x\mathcal{S}'}\lambda_D \simeq 0.2 \simeq 2k_{x\mathcal{L}}\lambda_D$ and $\omega/\omega_p \simeq 0.006$; at $\omega_p t = 4500$, $\mathcal{S}''$ waves appear, indicating the occurrence of the second decay cascade. At larger times (not shown here), low-frequency spectral energy mostly gathers toward smaller wavenumbers below 0.05; however, dispersion curves continue to exhibit the excitation of ion acoustic waves along the theoretical dispersion laws, but with no specific amplitude enhancements near $k_{\mathcal{S}'}$ and $k_{\mathcal{S}''}$. For a smaller $\Delta N = 0.025$, $\mathcal{S}'$ and $\mathcal{S}''$ waves can be more clearly identified (see Figure 4(f) at $\omega_p t = 1500$); the waves $\mathcal{S}'$ persist near $k_{\mathcal{S}'}\lambda_D \simeq 0.2$ up to late times ($\omega_p t = 11$, 500; Figure 4(g)), whereas the waves $\mathcal{S}''$ are no more visible.

All these features are in agreement with Figure 4(e), which shows the time variations of energies of ion acoustic and Langmuir waves, for $\Delta N = 0.025$ and $\Delta N = 0.05$. After reaching a maximum near $\omega_p t \simeq 1000$, the energy $W_{\mathcal{L}}$ slowly decreases, due to the formation of a tail of accelerated beam electrons resulting from Langmuir wave scattering on random density fluctuations (Krafft et al. 2013; Krafft & Savoini 2023). This effect is more prominent for larger ΔN than for smaller ones. The ion acoustic energy $W_{\mathcal{S}'}$, which is around 1 order of magnitude less than in the homogeneous plasma case, reaches its maximum at roughly the same time as the Langmuir backscattered waves' energy $W_{\mathcal{L}'}$, showing a correlation between them. During the saturation stage, $W_{\mathcal{L}'}$ and $W_{\mathcal{S}'}$ decrease with nearly the same rate, for both ΔN. One can conclude that ESD can occur and persist in a randomly homogeneous plasma, depending on the value of ΔN, and with significantly reduced energies of participating waves and scattering of their spectral and dispersion properties, compared to the homogeneous plasma case.

Spatial distributions of wave fields show that ESD only occurs in regions where the plasma density is quasi-uniform or depleted and the resonance conditions necessary for three-wave interaction can be met. Indeed, density fluctuations scatter randomly the waves out of resonance one with another. During time evolution, Langmuir wave energy mostly self-organizes outside regions of density humps (Krafft & Volokitin 2021), where interactions

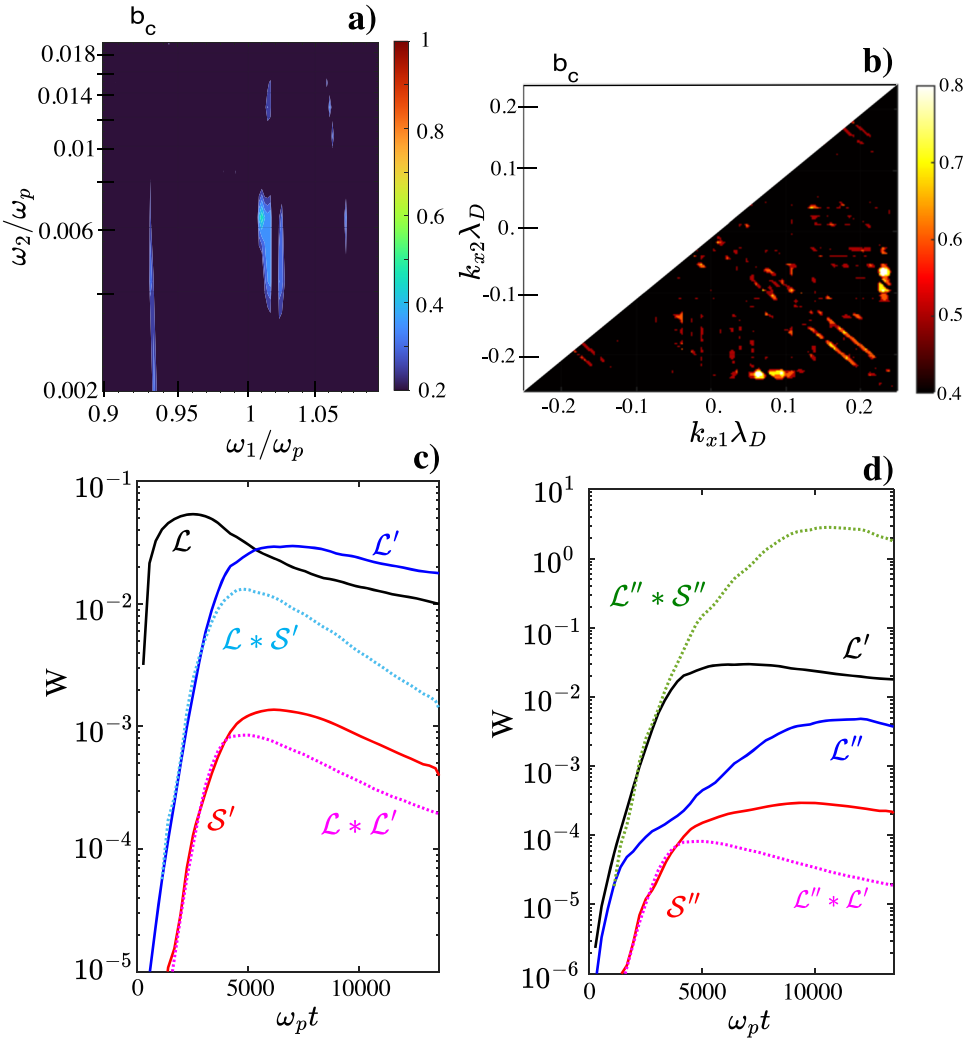

Figure 3. Homogeneous plasma with $T_e/T_i = 10$. (a) Cross-bicoherence b_c of the triplet (δn_i, E_x, E_y) in the plane (ω_1/ω_p, ω_2/ω_p), in logarithmic scales; the maximum is $b_c(\omega_1, \omega_2) = 0.5$, at $\omega_1/\omega_p = 0.006$ and $\omega_2/\omega_p = 1.014$. (b) Cross-bicoherence b_c of the triplet (δn_i, E_x, E_y) in the plane ($k_{x1}\lambda_D$, $k_{x2}\lambda_D$); the maximum is $b_c(k_{x1}, k_{x2}) = 0.86$, at $k_{x1}\lambda_D = 0.225$ and $k_{x2}\lambda_D = -0.096$. (c) Time variations of energies of Langmuir waves $\mathcal{L}$ and $\mathcal{L}'$ (black and blue) and ion acoustic modes $\mathcal{S}'$ (red), as well as of the energy products $W_{\mathcal{L}}W_{\mathcal{L}'}$ (dotted pink, $\mathcal{L} * \mathcal{L}'$) and $W_{\mathcal{L}}W_{\mathcal{S}'}$ (dotted light blue, $\mathcal{L} * \mathcal{S}'$). (d) Time variations of energies of Langmuir waves $\mathcal{L}'$ and $\mathcal{L}''$ (black and blue) and ion acoustic modes $\mathcal{S}''$ (red), as well as of the energy products $W_{\mathcal{L}''}W_{\mathcal{S}''}$ (dotted green, $\mathcal{L}'' * \mathcal{S}''$) and $W_{\mathcal{L}''}W_{\mathcal{L}'}$ (dotted pink, $\mathcal{L}'' * \mathcal{L}'$). (c)–(d) Energies, in logarithmic scales, are integrated on the 2D simulation box and normalized by the initial beam energy. All variables are dimensionless.

between incident and reflected (on density fluctuations) Langmuir waves can occur. Figures 4(h)–(i) show the joint time evolution of profiles (cross sections at fixed y) of the parallel electric field E_x and $\delta n_i/n_0$, for $1300 \lesssim \omega_p t \lesssim 3970$. The latter exhibits localized oscillations with wavelengths around 35–45λ_D (corresponding to $k_{x\mathcal{S}'}\lambda_D \sim 0.2 \simeq (2k_{x\mathcal{L}} - k_0)\lambda_D$, $k_{x\mathcal{S}''}\lambda_D \sim -0.18 \simeq (-2k_{x\mathcal{L}} + 3k_0)\lambda_D$) propagating with group velocities around c_s/v_T and $-c_s/v_T$, i.e., to forward and backward ion acoustic waves able to interact resonantly with Langmuir waves via ESD, whereas the former one shows, within the same time interval, the interaction of beam-driven and backscattered Langmuir waves, manifesting exactly in the plasma region where ion acoustic waves appear. This illustrates a decay process occurring in a localized region of the 2D simulation box, where plasma density is weakly perturbed by random fluctuations. To conclude, the plasma density turbulence has a strong impact on the dynamics of ESD, limiting its occurrence to regions of depleted or quasi-uniform plasma, where correlations between waves' phases and resonance conditions can be realized.

2.3. Influence of the Electron-to-ion Temperature Ratio

Let us now study the influence of the electron-to-ion temperature ratio T_e/T_i on ESD, by presenting firstly results obtained for the above homogeneous plasma, with $T_e/T_i = 1$ instead of $T_e/T_i = 10$.

The ratio $\gamma_{\mathcal{S}'}/\omega_{\mathcal{S}'}$ of the damping rate to the frequency of the ion acoustic waves $\mathcal{S}'$ (with $k_{x\mathcal{S}'}\lambda_D \sim 0.2$) can be estimated at $T_e/T_i = 1$ as (Gary 1993) $\gamma_{\mathcal{S}'}/\omega_{\mathcal{S}'} \simeq 0.48$ ($\gamma_{\mathcal{S}'} \simeq 0.002\omega_p$) and at $T_e/T_i = 10$ as $\gamma_{\mathcal{S}'}/\omega_{\mathcal{S}'} \simeq 0.03$ ($\gamma_{\mathcal{S}'} \simeq 0.00015\omega_p$). Thus, ion acoustic waves are heavily damped at $T_e = T_i$ and nonlinear induced scattering (NLIS) of Langmuir waves off ions, where thermal ions interact with the beat between a beam-driven and a backscattered Langmuir wave, becomes dominant over ESD (Tsytovich 1970). An ion acoustic quasi-mode $\mathcal{S}'_{qm}$ appears, which is a low-frequency beating between $\mathcal{L}$ and $\mathcal{L}'$ waves, with a phase velocity $\boldsymbol{v}_p$ satisfying $\boldsymbol{v}_p \cdot (\boldsymbol{k}_{\mathcal{L}} - \boldsymbol{k}_{\mathcal{L}'}) \simeq (\omega_{\mathcal{L}} - \omega_{\mathcal{L}'})$, that interacts nonlinearly with thermal ions. Further work on the NLIS at $T_e \lesssim T_i$ will be done in a forthcoming paper.

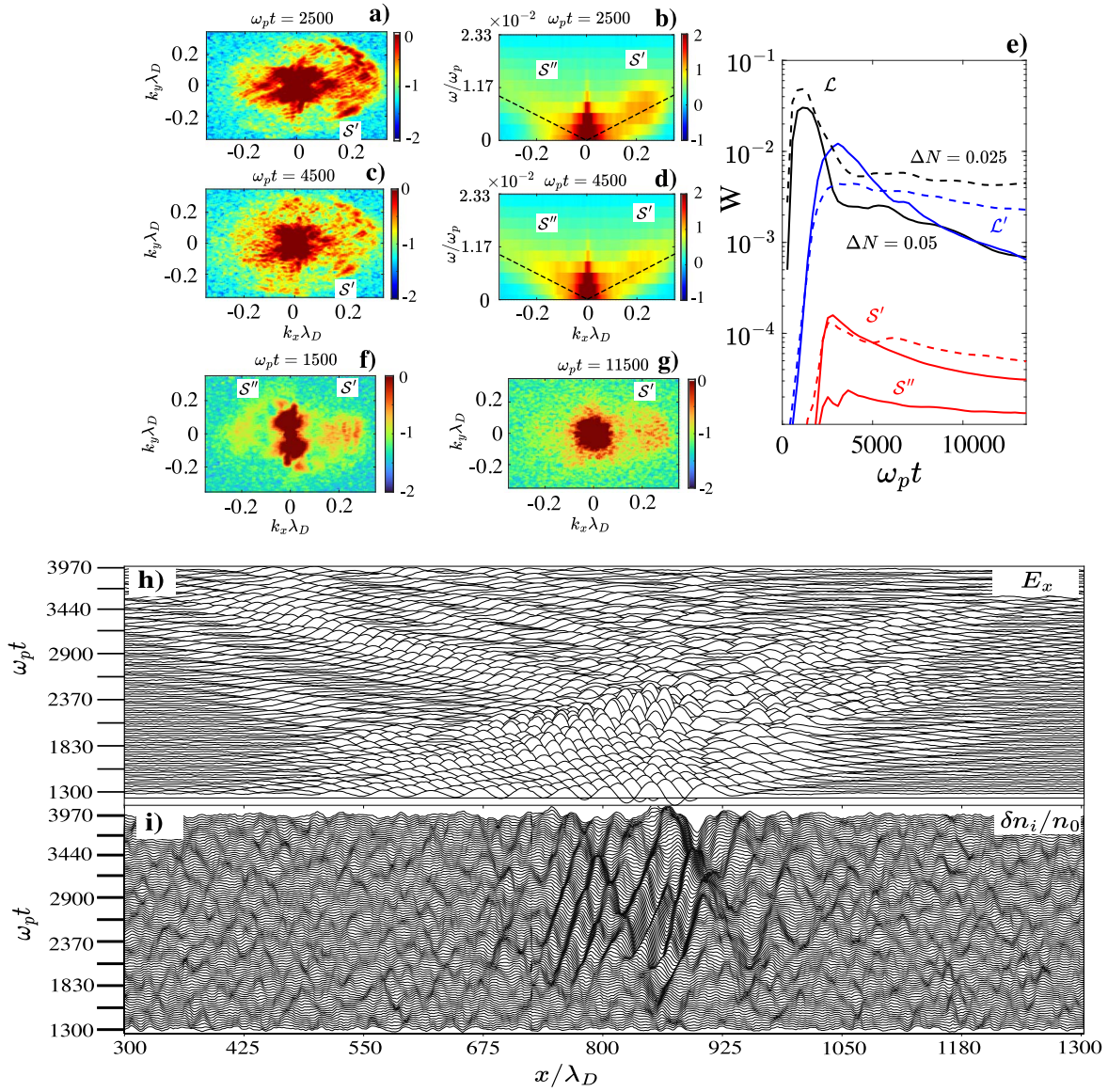

Figure 4. (For a better representation of (h) and (i), please zoom or print.) Randomly inhomogeneous plasma with $\Delta N > 0$ and $T_e/T_i = 10$. (a), (c) Energy spectra of ion acoustic waves $\mathcal{S}'$ and $\mathcal{S}''$ in the plane $(k_x\lambda_D, k_y\lambda_D)$, at $\omega_p t = 2500$ and 4500. (b), (d) Dispersion curves, at the same times, in the plane $(\omega/\omega_p, k_x\lambda_D)$; the black dashed lines represent the theoretical dispersion law; $\Delta N = 0.05$. (e) Variations with time of Langmuir and ion acoustic wave energies (integrated on the 2D simulation box and normalized by the initial beam energy), for $\Delta N = 0.05$ (solid lines) and $\Delta N = 0.025$ (dashed lines), in logarithmic scale. $\mathcal{L}$: black; $\mathcal{L}'$: blue; $\mathcal{S}'$, $\mathcal{S}''$: red. (f), (g) Ion acoustic energy spectra in the plane $(k_x\lambda_D, k_y\lambda_D)$, at $\omega_p t = 1500$ and 11,500, for $\Delta N = 0.025$. (h) Time evolution ($1300 \lesssim \omega_p t \lesssim 3970$) of profiles along x of the parallel electric field E_x. (i) Corresponding profiles of $\delta n_i/n_0$, in the same time interval as (h); ion acoustic waves propagate in the forward and backward directions (oblique lines with slopes c_s/v_T and $-c_s/v_T$). All variables are normalized.

Quasi-modes $\mathcal{S}'_{qm}$ with wavelengths around $35\lambda_D$ can be distinguished on the spatial distribution of $\delta n_i/n_0$ (Figure 5(a)), at $\omega_p t = 4500$, for $T_e/T_i = 1$ and $\Delta N = 0$. Moreover, in Figures 5(b)–(c), the low-frequency energy spectra show, at $\omega_p t = 2500$ ($\omega_p t = 4500$), quasi-modes $\mathcal{S}'_{qm}$ ($\mathcal{S}''_{qm}$) generated at $k_x \sim 0.2\lambda_D^{-1}$ ($k_x \sim -0.18\lambda_D^{-1}$). Note that these modes do not lie on the ion acoustic wave dispersion curves (Figures 5(d)–(e)) . We note that in Figures 5(c) a small amplitude excitation appears near $k_x \simeq -0.1\lambda_D^{-1}(\mathcal{S}_{qm})$, which is connected with another wave interaction process that will be studied in a companion paper.

Moreover, the time variations of high- and low-frequency energies show that (Figure 5(f)), whereas the waves $\mathcal{L}$ and $\mathcal{L}'$ present roughly the same behavior than at $T_e/T_i = 10$, the waves $\mathcal{L}''$ exhibit a significantly larger saturation amplitude at late times (compare with Figure 1(a)), indicating that another process than ESD is responsible for Langmuir wave generation. The energies of the ion acoustic quasi-modes $\mathcal{S}'_{qm}$ and $\mathcal{S}''_{qm}$ are reduced by more than 1 order of magnitude compared to the case with $T_e/T_i = 10$, and their growth rates are significantly decreased (compare the solid and dashed red lines in Figure 5(f)).

Finally, Figures 5(g)–(i) show the time variation of low-frequency energy spectra in a plasma with $\Delta N = 0.05$ and $T_e/T_i = 1$. Quasi-modes $\mathcal{S}'_{qm}$ and $\mathcal{S}''_{qm}$ appear near $\omega_p t \simeq 1500$, reach a maximum intensity at $\omega_p t \simeq 3000$, and are almost indiscernible from the ambient noise at $\omega_p t \gtrsim 4000$ (not shown here). Then, signatures of NLIS off ions can be observed in inhomogeneous solar wind regions with $T_e/T_i \sim 1$, but rarely, due to the modes' localization in plasma regions with quasi-uniform or reduced density only, and to the small intensity of the low-frequency quasi-modes.

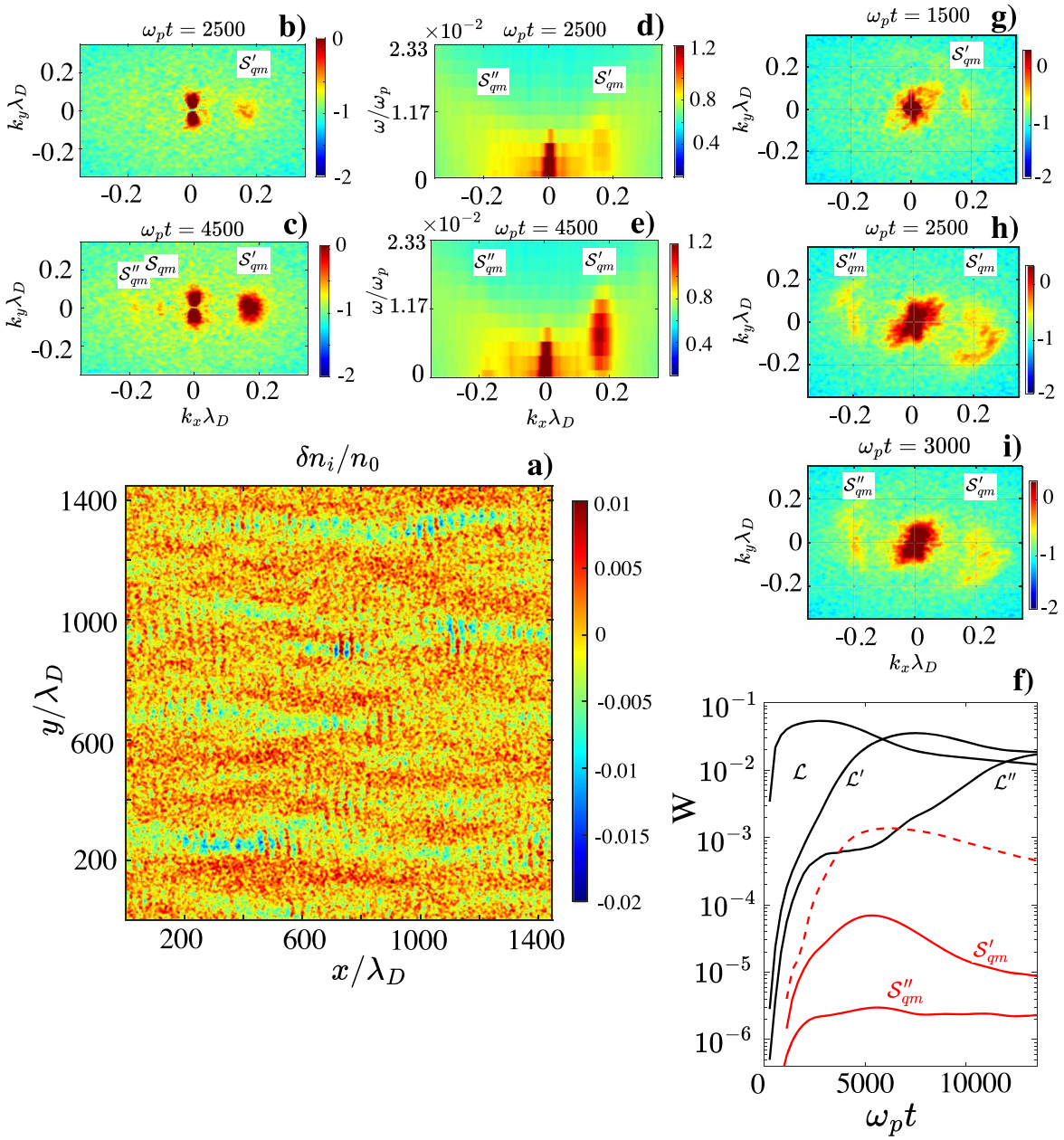

Figure 5. (a) Space distribution of $\delta n_i/n_0$, at $\omega_p t = 4500$, for a homogeneous plasma with $T_e/T_i = 1$. (b)–(c) Ion acoustic quasi-modes' $\mathcal{S}'_{qm}$ and $\mathcal{S}''_{qm}$ energy spectra in the plane ($k_x\lambda_D$, $k_y\lambda_D$), at $\omega_p t = 2500$ and 4500, for $\Delta N = 0$ and $T_e/T_i = 1$, in logarithmic scales. (d)–(e) Dispersion curves corresponding to (b)–(c). (f) Time variations of energies (integrated on the 2D simulation box and normalized by the initial beam energy) of Langmuir waves $\mathcal{L}$, $\mathcal{L}'$, and $\mathcal{L}''$ (black) and ion acoustic quasi-modes $\mathcal{S}'_{qm}$ and $\mathcal{S}''_{qm}$ (solid red), in logarithmic scale, for $\Delta N = 0$ and $T_e/T_i = 1$; for comparison, the dashed red line is the energy variation of the $\mathcal{S}'$ mode for $\Delta N = 0$ and $T_e/T_i = 10$. (g)–(i) Ion acoustic quasi-modes' energy spectra in the plane ($k_x\lambda_D$, $k_y\lambda_D$), at $\omega_p t = 1500$, 2500, and 4500, for $\Delta N = 0.05$ and $T_e/T_i = 1$. All variables are normalized.

3. Conclusion

The dynamics of nonlinear electrostatic wave–wave interactions, studied first in a homogeneous plasma where Langmuir wave turbulence is generated by a type III electron beam and ion acoustic waves are weakly damped ($T_e/T_i \sim 10$), show that the dominant nonlinear three-wave process is ESD, which is also the source of backscattered Langmuir waves. This conclusion is also valid for solar wind regions with $3 \lesssim T_e/T_i \lesssim 10$—where ion acoustic waves are moderately damped—and with very low levels of density turbulence (quasi-homogeneous plasmas). This result was obtained owing to challenging 2D PIC simulations, which allowed us for the first time to study in detail the 2D dynamics of low-frequency waves and to demonstrate the occurrence of ESD generated by type III beams in the solar wind. Furthermore, in solar wind plasmas where the electron-to-ion temperature ratio reaches values down to $1 \lesssim T_e/T_i \lesssim 3$, with heavily damped ion acoustic waves ($\gamma_{\mathcal{S}}/\omega_{\mathcal{S}} \simeq 0.17$–$0.48$), simulations show that NLIS off ions leads to Langmuir waves' growth and amplitudes close to those of ESD—with some small differences however—and to small amplitude ion acoustic quasi-modes.

For inhomogeneous plasmas with random density fluctuations of average levels of several percent of the ambient density, both ESD and NLIS processes can only arise in localized plasma regions of reduced or quasi-uniform density, where Langmuir

waves' energy accumulates during their scattering on the density humps. Moreover, Langmuir wave turbulence, which generates at early times emission of fundamental electromagnetic waves via linear conversion, is decaying with time due to the formation of a tail of accelerated beam electrons caused by Langmuir waves' scattering on density fluctuations; then, the energy available for further ESD or NLIS, which due to their nonlinear character arise later, is reduced.

Due to the combined action of heavy ion acoustic waves' damping at $1 \lesssim T_e/T_i \lesssim 3$ and Langmuir wave scattering on random density fluctuations, the occurrence rate of ESD can be significantly reduced in favor of NLIS, so that, in certain conditions, it should not be easy to detect it by satellites in the solar wind near 1 au. Nevertheless, one can expect to observe it in regions where the plasma density is weakly perturbed by low-frequency turbulence and the temperature ratio satisfies $T_e \gtrsim 3T_i$. Finally, the Doppler-shifted double-peak structures commonly observed by spacecraft in the solar wind and exhibiting two Langmuir waves with close frequencies, usually attributed to ESD, could also result from interactions of Langmuir waves with density fluctuations, as reflections off density gradients or scattering at a range of angles, for example, or to NLIS on ions.

Acknowledgments

This work was granted access to the HPC resources of TGCC and under the allocation 2023-A0130510106 made by GENCI. This project was also provided with computer and storage resources by GENCI at CINES thanks to the special access grand challenge 2023—gda2212 on the supercomputer Adastra's MI2050x partition. C.K. acknowledges the "Programme National Soleil Terre" (PNST), the Centre National d'Etudes Spatiales (CNES, France) and the Institut Universitaire de France (IUF).

ORCID iDs

C. Krafft https://orcid.org/0000-0002-8595-4772

References

Cairns, I. H., & Robinson, P. A. 1992, GeoRL, 19, 2187
Celnikier, L. M., Muschietti, L., & Goldman, M. V. 1987, A&A, 181, 138
Dakeyo, J.-B., Maksimovic, M., Démoulin, P., Halekas, J., & Stevens, M. L. 2022, ApJ, 940, 130
Derouillat, J., Beck, A., Pérez, F., et al. 2017, CoPhC, 222, 351
Gary, S. P. 1993, Theory of Space Plasma Microinstabilities (Cambridge: Cambridge Univ. Press)
Graham, D. B., & Cairns, I. H. 2013, JGRA, 118, 3968
Gurnett, D. A., Hospodarsky, G. B., Kurth, W. S., Williams, D. J., & Bolton, S. J. 1993, JGRA, 98, 5631
Gurnett, D. A., Maggs, J. E., Gallagher, D. L., Kurth, W. S., & Scarf, F. L. 1981, JGR, 86, 8833
Henri, P., Briand, C., Mangeney, A., et al. 2009, JGRA, 114, A03103
Hospodarsky, G. B., & Gurnett, D. A. 1995, GeoRL, 22, 1161
Kellogg, P. J., Goetz, K., Monson, S. J., & Bale, S. D. 1999, JGR, 104, 17069
Kellogg, P. J., Goetz, K., Monson, S. J., & Opitz, A. 2013, JGRA, 118, 4766
Kim, Y. C., & Powers, E. J. 1979, ITPS, 7, 120
Kontar, E. P., & Pécseli, H. L. 2002, PhRvE, 65, 066408
Krafft, C., & Savoini, P. 2021, ApJL, 917, L23
Krafft, C., & Savoini, P. 2022, ApJL, 924, L24
Krafft, C., & Savoini, P. 2023, ApJ, 949, 24
Krafft, C., & Volokitin, A. S. 2021, ApJ, 923, 103
Krafft, C., Volokitin, A. S., & Gauthier, G. 2019, Fluids, 4, 69
Krafft, C., Volokitin, A. S., & Krasnoselskikh, V. V. 2013, ApJ, 778, 111
Krafft, C., Volokitin, A. S., & Krasnoselskikh, V. V. 2015, ApJ, 809, 176
Krasnoselskikh, V. V., Dudok de Wit, T., & Bale, S. D. 2011, AnGeo, 29, 613
Krasnoselskikh, V. V., Lobzin, V. V., Musatenko, K., et al. 2007, JGRA, 112, A10109
Krupar, V., Kontar, E. P., Soucek, J., et al. 2015, A&A, 580, A137
Krupar, V., Szabo, A., Maksimovic, M., et al. 2020, ApJS, 246, 57
Li, B., Willes, A. J., Robinson, P. A., & Cairns, I. H. 2003, PhPl, 10, 2748
Melrose, D. B. 1986, Instabilities in Space and Laboratory Plasmas (Cambridge: Cambridge Univ. Press)
Nishikawa, K. I., & Cairns, I. H. 1991, JGR, 96, 19343
Reid, H. A. S., & Ratcliffe, H. 2014, RAA, 14, 773
Robinson, P. A., Cairns, I. H., & Willes, A. J. 1994, ApJ, 422, 870
Robinson, P. A., Willes, A. J., & Cairns, I. H. 1993, ApJ, 408, 720
Sauer, K., Malaspina, D. M., Pulupa, M., & Salem, C. S. 2017, JGRA, 122, 7005
Soucek, J., Krasnoselskikh, V., Dudok de Wit, T., Pickett, J., & Kletzing, C. 2005, JGRA, 110, A08102
Tsytovich, V. N. 1970, Nonlinear Effects in Plasma (New York: Plenum Press)
Umeda, T., & Ito, T. 2008, PhPl, 15, 084503
Volokitin, A. S., & Krafft, C. 2018, ApJ, 868, 104
Willes, A. J., Bale, S. D., & Cairns, I. H. 2002, JGRA, 107, 1320
Wilson, L. B., Stevens, M. L., Kasper, J. C., et al. 2023, ApJS, 269, 62
Ziebell, L. F., Yoon, P. H., Petruzzellis, L. T., Gaelzer, R., & Pavan, J. 2015, ApJ, 806, 237